

Accelerated Stochastic Quasi-Newton Optimization on Riemann Manifolds

Anirban Roychowdhury, Srinivasan Parthasarathy
Department of Computer Science and Engineering
The Ohio State University

roychowdhury.7@osu.edu, srini@cse.ohio-state.edu

October 13, 2021

Abstract

We propose L-BFGS and trust-region algorithms on Riemann manifolds that use stochastic variance reduction techniques to speed up convergence. For the stochastic L-BFGS algorithm we analyze and prove linear convergence rates for geodesically convex problems on the manifold, without resorting to linesearch methods designed to satisfy Wolfe conditions on the step size. To the best of our knowledge our trust-region method with stochastic variance reduction techniques is the first of its kind in the literature. We conduct experiments on Karcher mean computation for positive definite matrices and computation of leading eigenvectors for both synthetic and real data matrices, and demonstrate notably better performance than recently-proposed first-order stochastic optimization methods on Riemann manifolds, as well as standard trust-region manifold optimization techniques.

1 Introduction

Optimization algorithms are a mainstay in machine learning research, underpinning recent research ranging from linear regression and SVMs to deep learning. Consequently, scaling such algorithms to large scale datasets while preserving theoretical guarantees is of paramount importance. Convex optimization problems admit scalable stochastic algorithms [9], but adding constraints on the search space usually lead to unpredictable convergence behavior. One approach to handling such constrained optimization problems on vector spaces (usually Euclidean) is to reformulate them as optimization tasks on a suitable Riemannian manifold, with the constraints acting as manifold parametrization. Often, the problems can be shown to be convex with respect to geodesics on the manifold, leading to provably efficient optimization algorithms. These ideas can then be combined with stochastic optimization techniques [5] influenced by [19], to deal with large datasets with theoretical convergence guarantees.

In the Euclidean setting, one can show quadratic convergence rates for convex problems using Newton iterations, but these tend to be prohibitively expensive in high-

dimensional big-data settings due to the need to store and invert the Hessian matrix. This limitation has led to the development of quasi-Newton methods, most notably L-BFGS [14], which uses lower-order terms to approximate the (inverse) Hessian. The curvature information provided by the Hessian estimate allows superlinear convergence in ideal settings [16]. In contrast, most stochastic optimization algorithms in the literature are modifications of first order gradient-descent [7, 8] with sublinear convergence in most practical situations. To improve convergence rates by incorporating curvature information, researchers have been investigating stochastic variants of quasi-Newton methods [10]. One such Euclidean variant of L-BFGS has recently been combined with variance reduction techniques and shown to have a linear convergence rate in the stochastic setting [15]. However, such methods are notably suboptimal for non-convex loss functions, where even asymptotic convergence cannot be guaranteed. One approach in these cases is to use rank-one updates for the inverse Hessian in a quasi-Newton scheme, with trust-region techniques employed to solve a local quadratic approximation of the objective function (e.g. SR1 methods and variants) [2, 16].

Variance reduction techniques are a parallel development in the optimization literature, that aims to improve convergence rates of stochastic algorithms by explicitly reducing the variance of gradient estimates [12, 20]. A nice advantage of this technique is the removal of the dependence on decaying learning rates for proving convergence. Choosing an effective decay for the step sizes is a nontrivial issue when applying SGD and related algorithms within large-scale optimization scenarios.

The presence of constraints on the search space can further challenge optimization algorithms possibly leading to convergence difficulties for numerical algorithms, for example the unit-norm constraint for computing leading eigenvectors in the PCA setting [20]. Projection-based strategies can alleviate this to some extent [17], but alternating between solving and projecting can be prohibitively expensive in high dimensions. A method to unconstrain such problems is Riemannian optimization, where the Euclidean constraints are used to cast the problem onto a suitable Riemann manifold. The unit-norm constraint, for instance, can be used to cast the eigenvector problem into an unconstrained version on the unit sphere, which happens to be one of the most well-behaved Riemann manifolds. Algorithms for unconstrained optimization on Riemann manifold often use Riemann geometry cues to define notions of convexity on the manifold, in order to prove convergence. However, note that the convergence speed limitations of unconstrained stochastic algorithms in the Euclidean case apply here as well; for instance a straightforward port of SGD to Riemann manifolds will suffer from the same sublinear convergence seen in Euclidean space. To remedy this, researchers have begun investigating the use of the variance reduction techniques alluded to earlier, in the manifold setting [22].

Contributions: Here we focus on finite-sum optimization (empirical risk minimization) problems of the form:

$$\min_{x \in \mathcal{M}} f(x) = \frac{1}{N} \sum_{i=1}^N f_i(x), \quad (1)$$

where \mathcal{M} denotes a suitable Riemann manifold, and the functions $f_i : \mathcal{M} \rightarrow \mathbb{R}$ are assumed to be smooth on the manifold. Definitions of convexity, smoothness and other

necessary concepts on the manifold are straightforward extensions of the standard Euclidean baselines, and are provided in §2. We extend recent work on Riemann optimization by proposing two stochastic quasi-Newton optimization algorithms on manifolds with explicit variance reduction techniques, and analyze their behavior for a couple of different optimization problems. To the best of our knowledge, we are the first to develop and analyze variance reduction techniques for quasi-Newton optimization on manifolds. Moreover, our second algorithm, based on an accelerated trust regions technique, shows strong performance compared to both existing stochastic manifold optimization methods, as well as the standard Riemannian trust-regions technique, on our synthetic and real data experiments.

2 Preliminaries

2.1 Riemannian geometry

We begin with a brief overview of the differential geometric concepts we use in this work. We consider C^∞ (smooth) manifolds that are locally homeomorphic to open subsets of \mathbb{R}^D , in the sense that the neighborhood of each point can be assigned a system of coordinates of appropriate dimensionality. Formally, this is defined with the notion of a *chart* $c : U \rightarrow \mathbb{R}^D$ at each $x \in \mathcal{M}$, where $U \subset \mathcal{M}$ is an open subspace containing x . Smooth manifolds are ones with covering collections of differentiable (C^∞) charts. A *Riemannian metric* $g(\cdot, \cdot)$ is a bilinear C^∞ tensor field of type $\binom{0}{2}$, that is also symmetric and positive definite. A manifold endowed with such a metric is called a Riemannian manifold. The tangent space $T_x\mathcal{M}$ at every $x \in \mathcal{M}$ is a vector space, with the Riemannian metric $g : T_x\mathcal{M} \times T_x\mathcal{M} \rightarrow \mathbb{R}$ as the attendant metric. g therefore induces a norm for vectors in the tangent space, which we denote by $\|\cdot\|$.

The Levi-Civita connection induces the notion of parallel transport of vectors from one tangent space to another along a geodesic, in a metric preserving way. That is, we have an operator $\Gamma_\gamma : T_x\mathcal{M} \rightarrow T_y\mathcal{M}$ where, informally speaking, γ joins x and y , and for any $u, \nu \in T_x\mathcal{M}$, we have $g(u, \nu) = g(\Gamma(u), \Gamma(\nu))$. The parallel transport can be shown to be an isometry.

For every smooth curve $\gamma : [0, 1] \rightarrow \mathcal{M}$ lying in \mathcal{M} , we denote its velocity vector as $\dot{\gamma}(t) \in T_x\mathcal{M}$ for each $t \in [0, 1]$, with the “speed” given by $\|\dot{\gamma}(t)\|$. The length of such a curve is usually measured as $L(\gamma) = \int_0^1 \|\dot{\gamma}(t)\| dt$. Denoting the covariant derivative along γ of some $\nu \in T_x\mathcal{M}$, with respect to the Riemannian (Levi-Civita) connection, by $A\nu$, we call $A\dot{\gamma}$ the *acceleration* of the curve. Curves with constant velocities ($A\dot{\gamma} \equiv 0$) are called *geodesics*, and can be shown to generalize the notion of Euclidean straight lines.

We assume that every pair $x, y \in \mathcal{M}$ can be connected by a geodesic γ s.t. $\gamma(0) = x$ and $\gamma(1) = y$. Immediately we have the notion of “distance” between any $x, y \in \mathcal{M}$ as the minimum length of all geodesics connecting x and y . Note the distinction from Euclidean geometry, where one can only have a single “shortest” path between any two points, i.e. the straight line. The surface of a sphere, for instance, is a Riemannian manifold, and indeed there are infinitely many geodesics between any two points on

the sphere, all of the same length.

The geodesic induces a useful operator called the *exponential map*, defined as $\text{Exp}_x : T_x\mathcal{M} \rightarrow \mathcal{M}$ s.t. $\text{Exp}_x(\nu) = \gamma(1)$ where $\gamma(0) = x, \gamma(1) = y$ and $\dot{\gamma}(0) = \nu$. If there is a unique geodesic connecting x and y , then the exponential map has an inverse, denoted by $\text{Exp}_x^{-1}(y)$. The length of the geodesic can of course be seen to be $\|\text{Exp}_x^{-1}(y)\|$.

The derivative D of a differentiable function is defined using the Riemannian connection by the following equivalence: $Df(x)\nu = \nu f$, where $\nu \in T_x\mathcal{M}$. Then, by the Riesz representation theorem, there exists a gradient $\nabla f(x) \in T_x\mathcal{M}$ s.t. $\forall \nu \in T_x\mathcal{M}, Df(x)\nu = g_x(\nabla f(x), \nu)$. Similarly, we can denote the Hessian as follows: $D^2f(x)(\cdot, \cdot) : T_x\mathcal{M} \times T_x\mathcal{M} \rightarrow \mathbb{R}$. We denote the mapping from $\nu \in T_x\mathcal{M}$ to the Riesz representation of $D^2f(x)(\nu, \cdot)$ by $\nabla^2 f(x)$. One can consult standard textbooks on differential geometry [6, 13] for more details.

2.2 Convexity and Lipschitz smoothness on manifolds

We define manifold (or geodesic) convexity concepts analogous to the Euclidean base-lines, as follows [11, 21]: a set $U \subset \mathcal{M}$ is convex on the manifold if $\forall x, y \in U$, there exists a geodesic γ connecting x, y that completely lies in U , i.e. $\gamma(0) = x, \gamma(1) = y$. Then, a function can be defined as convex w.r.t. geodesics if $\forall x, y \in U$ where $\exists \gamma$ connecting x, y on the manifold, we have:

$$f(\gamma(t)) \leq tf(x) + (1-t)f(y) \quad \forall t \in [0, 1].$$

We can also define a notion of strong convexity as follows [22]: a function is called S -strongly convex if for any $x, y \in U$ and (sub)gradient ∇_x , we have

$$f(y) \geq f(x) + g_x(\nabla_x, \text{Exp}_x^{-1}(y)) + \frac{S}{2} \|\text{Exp}_x^{-1}(y)\|^2. \quad (2)$$

We define Lipschitz smoothness of a function by imposing Lipschitz continuity on the gradients, as follows: $\forall x, y \in U$,

$$\|\nabla(x) - \Gamma_\gamma \nabla(y)\| \leq L \|\text{Exp}_x^{-1}(y)\|,$$

L being the smoothness parameter. analogous to the Euclidean case, this allows us to formulate Lipschitz smoothness of f by the following condition:

$$f(y) \leq f(x) + g_x(\nabla_x, \text{Exp}_x^{-1}(y)) + \frac{L}{2} \|\text{Exp}_x^{-1}(y)\|^2.$$

3 Stochastic Riemannian L-BFGS

We present a stochastic L-BFGS algorithm on Riemann manifolds and analyze the convergence behavior for convex and nonconvex differentiable functions. We assume the manifolds to be smooth, with existence of unique distance-minimizing geodesics between every two points, which allows us to have a well-defined inverse exponential map. For simplicity, we also assume f to have a unique minimum at $x^* \in U$, where

U is a compact convex subset of the manifold. Additional / equivalent assumptions on certain properties of the manifold or operations in the algorithm will be introduced on an as-needed basis in the subsequent sections.

3.1 The Algorithm

The pseudocode is shown in Algorithm 1. We provide a brief discussion of the salient properties, as well as comparisons with similar algorithms in the Euclidean domain, for example [10, 15], as well as those on Riemann manifolds, for example [21]. To begin, note that ∇ denotes the Riesz representation of the gradient D , as defined in §2.1. We denote full gradients by ∇ and stochastic gradients by $\tilde{\nabla}$. Similar to other stochastic algorithms with variance-reduction, we use two loops: each iteration of the inner loop corresponds to drawing one minibatch from the data and performing the stochastic gradient computations (lines 8,9), whereas each outer loop iteration corresponds to two passes over the full dataset, once to compute the full gradient (line 6) and the other to make multiple minibatch runs (lines 7 through 20). Compared to the Euclidean setting, note that the computation of the variance-reduced gradient in line 10 involves an extra step: the gradients ($\nabla f(x)$ -s) reside in the tangent space, therefore we have to perform parallel transport to bring them to the same tangent space before performing linear combinations.

We also observed more robust behavior from the extra minibatching step in line 14 over using a single minibatch (as in [21] for instance) to compute the correction pairs for the Hessian update, similar to [10]. To avoid memory issues and complications arising from Hessian-vector computations in the Riemann setting, we chose to update the second correction variable $y_r = \tilde{\nabla} f(u_r) - \Gamma_\gamma \tilde{\nabla} f(u_{r-1})$, instead of $\tilde{\nabla}^2 f(u_r) z_r$. We should note here that the parallel transport parametrization should be clear from the context; Γ_γ here denotes transporting the vector $\tilde{\nabla} f(u_{r-1}) \in T_{u_{r-1}} \mathcal{M}$ to $T_{u_r} \mathcal{M}$ along the connecting geodesic. We omit any relevant annotations for the transport symbol to prevent notational overload.

Once the corrections pairs s_r, z_r have been computed, computing the product of the inverse Hessian (approximation) with the variance reduced gradient in line 18 is performed using the standard two-loop recursion formula given in [16]. Note that we use a fixed stepsize in the update step, and do not impose or perform calculations designed to have it satisfy Armijo or Wolfe conditions. Of course, one could augment this algorithm with an appropriate linesearch procedure to possibly gain superlinear convergence, but we do not investigate this alternative here. However, this might help alleviate some of the issues encountered in our experiments, where the algorithm seems to get stuck in local modes after performing relatively well for the first few epochs, for a wide range of stepsizes. This behavior is in contrast to that for a similar algorithm in the Euclidean case [15]; the latter has been shown to perform quite robustly for both convex and nonconvex optimization problems on real datasets for a range of stepsizes. We intend to investigate this discrepancy in future work.

Algorithm 1 Stochastic VR-Riemannian L-BFGS

```

1: Input: Initial value  $x^0$ , parameters  $M$  and  $R$ , learning rate  $\eta$ , batch sizes  $b_m$  and  $b_r$ .
2: for  $s = 0, 1, \dots$  do
3:   Set  $x_0^{s+1} = x^s$ ;
4:   Set  $r = 0$ ;
5:   Initialize  $H_0$ ;
6:   Compute full gradient  $g^{s+1} = N^{-1} \sum_{i=1}^N \nabla f_i(x^s)$ ;
7:   for  $t = 0, 1, \dots, m - 1$  do
8:     Sample minibatch  $I_{b_m} \subset 1, \dots, N$ ;
9:     Compute  $\tilde{\nabla} f(x_t^{s+1})$  and  $\tilde{\nabla} f(x^s)$  using  $I_{b_m}$ ;
10:    Set  $\nu_t^{s+1} = \tilde{\nabla} f(x_t^{s+1}) - \Gamma_\gamma(\tilde{\nabla} f(x^s) - g^{s+1})$ ;
11:    Set  $x_{t+1}^{s+1} = \text{Exp}_{x_t^{s+1}}(-\eta H_r^{s+1} \nu_t^{s+1})$ ;
12:    if  $t \equiv 0 \pmod R$  then
13:      Set  $r = r + 1$ ;
14:      Sample minibatch  $I_{b_r} \subset 1, \dots, N$ ;
15:      Set  $u_r^{s+1} = R^{-1} \sum_{k=t-R}^{t-1} x_k^{s+1}$ ;
16:      Compute  $z_r^{s+1} = u_r^{s+1} - u_{r-1}^{s+1}$ ;
17:      Compute  $y_r^{s+1} | I_{b_r} = \tilde{\nabla} f(u_r^{s+1}) - \Gamma_\gamma \tilde{\nabla} f(u_{r-1}^{s+1})$ ;
18:      Update  $H_r^{s+1}$  as mentioned in the text;
19:    end if
20:  end for
21:  Set  $x^{s+1} = x_j^{s+1}$ ,  $j$  chosen randomly from  $1, \dots, m$ ;
22: end for

```

3.2 Analysis of convergence

The convergence discussion follows the standard template for L-BFGS algorithms in the literature [10, 16, 18]. We begin by stating the assumptions necessary for our proof of convergence.

Assumption 1. The function f in (1) is strongly convex on the manifold, whereas the f_i s are individually convex.

Assumption 2. There exist $\lambda, \Lambda \in (0, \infty)$, $\lambda < \Lambda$ s.t.

$$\lambda \|\nu\|_x^2 \leq D^2 f \leq \Lambda \|\nu\|_x^2 \quad \forall \nu \in T_x \mathcal{M}.$$

These two assumptions guarantee that f has a unique minimizer x^* in the convex sub-level set U .

Note the following BFGS update equation for the Hessian approximation:

$$\hat{B}_r = \Gamma_\gamma \left[\hat{B}_{r-1} - \frac{B_{r-1}(s_{r-1}, \cdot) \hat{B}_{r-1} s_{r-1}}{B_{r-1}(s_{r-1}, s_{r-1})} \right] \Gamma_\gamma^{-1}, \quad (3)$$

and by the Sherman-Morrison-Woodbury lemma, that of the inverse:

$$H_r = \Gamma_\gamma \left[G^{-1} H_{r-1} G + \frac{g_{x_{r-1}}(s_{r-1}, \cdot) s_{r-1}}{y_{r-1} s_{r-1}} \right] \Gamma_\gamma^{-1},$$

where $G = I - \frac{g_{x_{r-1}}(s_{r-1}, \cdot) \hat{y}_{r-1}}{y_{r-1} s_{r-1}}$.

3.2.1 Trace and determinant bounds

The assumptions above allow us to derive the following bounds on the trace and determinant of the inverse Hessian approximation H_r^{s+1} in the algorithm:

Lemma 3.3. *Let $B_r^{s+1} = (H_r^{s+1})^{-1}$ be the approximation of the Hessian generated by Algorithm 1, and \hat{B}_r^{s+1} and \hat{H}_r^{s+1} be the corresponding Lax-Milgram representations. Let M , the memory parameter, be the number of correction pairs used to update the inverse Hessian approximation. Then, under Assumptions 1 and 2, we have:*

$$\begin{aligned} \text{tr}(\hat{B}_r^{s+1}) &\leq \text{tr}(\hat{B}_0^{s+1}) + M\Lambda, \\ \det(\hat{B}_r^{s+1}) &\geq \det(\hat{B}_0^{s+1}) \frac{\lambda^M}{(\text{tr}(\hat{B}_0^{s+1}) + \Lambda M)^M}. \end{aligned}$$

Also,

$$\gamma I \preceq \hat{H}_r^{s+1} \preceq \Gamma I$$

for some $\Gamma \geq \gamma > 0$.

We should mention here that the symbols γ, Γ here have no relation to geodesics or parallel transport on the manifold.

Proof Sketch. The proof for the Euclidean case [10] can be generalized to the Riemannian scenario in a straightforward way. Using the L-BFGS update (3), we can bound the trace of the Lax-Milgram representation of the Hessian approximations as follows:

$$\text{tr}(\hat{B}_r) \leq \text{tr}(B_0) + M\Lambda.$$

This therefore proves boundedness of the largest eigenvalue of the \hat{B}_r estimates.

Similarly, to get a lower bound for the minimum eigenvalue, we bound the determinant as follows:

$$\det(\hat{B}_r) \geq \det(B_0) \frac{\lambda^M}{(\text{tr}(B_0) + M\Lambda)^M}.$$

The bounds on the maximum and minimum eigenvalues of B_r thus derived allows us to infer corresponding bounds for those of H_r as well, since by definition $H_r = \hat{B}_r^{-1}$. The derivation details are provided in the supplementary.

Proof. For brevity of notation we temporarily drop the $(s + 1)$ superscript. The proof for the Euclidean case [10] can be generalized to the Riemannian scenario in a straightforward way, as follows. Define the average Hessian G_r by

$$G_r(\cdot, \cdot) = \int_0^1 D^2[f(tz_r)](\cdot, \cdot) dt,$$

such that $y_r = G_r(z_r, \cdot)$. Then, it can be easily shown that G_r satisfies the bounds in Assumption 2. Furthermore, we have the following useful inequalities

$$\frac{y_r z_r}{\|z_r\|^2} = \frac{G_r(s_r, s_r)}{\|z_r\|^2} \geq \lambda, \quad \frac{\|y_r\|^2}{y_r z_r} \leq \Lambda. \quad (4)$$

Let \hat{y}_r be the Riesz representation of y_r . Recall that parallel transport is an isometry along the unique geodesics, which implies invariance of the trace operator. Then using the L-BFGS update (3) and (4), we can bound the trace of the Lax-Milgram representation of the Hessian approximations as follows:

$$\begin{aligned} \text{tr}(\hat{B}_r) &= \text{tr}(\Gamma_\gamma \hat{B}_{r-1} \Gamma_\gamma^{-1}) - \frac{\|\Gamma_\gamma \hat{B}_{r-1} s_{r-1}\|^2}{B_{r-1}(s_{r-1}, s_{r-1})} + \frac{\|\Gamma_\gamma \hat{y}_{r-1}\|^2}{y_{r-1} s_{r-1}} \\ &\leq \text{tr}(\Gamma_\gamma \hat{B}_{r-1} \Gamma_\gamma^{-1}) + \frac{\|\Gamma_\gamma \hat{y}_{r-1}\|^2}{y_{r-1} s_{r-1}} \\ &\leq \text{tr}(B_0) + M\Lambda. \end{aligned}$$

This therefore proves boundedness of the largest eigenvalue of the \hat{B}_r estimates.

Similarly, to get a lower bound for the minimum eigenvalue, we bound the determinant as follows:

$$\begin{aligned} \det(\hat{B}_r) &= \det(\Gamma_\gamma B_{r-1} \Gamma_\gamma^{-1}) \cdot \det\left(I - \frac{\hat{B}_{r-1} s_{r-1} s_{r-1}}{B_{r-1}(s_{r-1}, s_{r-1})}\right. \\ &\quad \left. + \frac{\hat{B}_{r-1}^{-1} y_{r-1} y_{r-1}}{y_{r-1} s_{r-1}}\right) \\ &= \det(\Gamma_\gamma B_{r-1} \Gamma_\gamma^{-1}) \frac{y_{r-1} s_{r-1}}{B_{r-1}(s_{r-1}, s_{r-1})} \\ &= \det(\Gamma_\gamma B_{r-1} \Gamma_\gamma^{-1}) \frac{y_{r-1} s_{r-1}}{\|s_{r-1}\|^2} \cdot \frac{\|s_{r-1}\|^2}{B_{r-1}(s_{r-1}, s_{r-1})} \\ &\geq \det(\Gamma_\gamma B_{r-1} \Gamma_\gamma^{-1}) \frac{\lambda}{\lambda_{\max}(B_{r-1})}, \end{aligned}$$

where we use λ_{\max} to denote the maximum eigenvalue of B_{r-1} , and use (4). Since λ_{\max} is bounded above by the trace of (\hat{B}_r) , we can telescope the inequality above to get

$$\det(\hat{B}_r) \geq \det(B_0) \frac{\lambda^M}{(\text{tr}(B_0) + M\Lambda)^M}.$$

The bounds on the maximum and minimum eigenvalues of B_r thus derived allows us to infer corresponding bounds for those of H_r as well, since by definition $H_r = \hat{B}_r^{-1}$. \square

3.3.1 Convergence results

Next we provide a brief overview of the bounds necessary to prove our convergence result. First, note the following bound implied by the Lipschitz continuity of the gradients:

$$\begin{aligned} & f(x_{t+1}^{s+1}) \\ & \leq f(x_t^{s+1}) + g(\nabla f(x_t^{s+1}), \text{Exp}_{x_t^{s+1}}^{-1}(x_{t+1}^{s+1})) \\ & \quad + \frac{L}{2} \|\text{Exp}_{x_t^{s+1}}^{-1}(x_{t+1}^{s+1})\|^2. \end{aligned}$$

Note the update step from line 11 of Algorithm 1: $x_{t+1}^{s+1} = \text{Exp}_{x_t^{s+1}}(-\eta H_r^{s+1} \nu_t^{s+1})$. We can replace the inverse exponential map in the inner product above by the quantity in the parentheses. In order to replace H_r^{s+1} by the eigen-bounds from Lemma 3.3, we invoke the following result (Lemma 5.8 from [13]):

Lemma 3.4. *For any $D \in T_x \mathcal{M}$ and $c, t \in \mathbb{R}$, $\gamma_{cD}(t) = \gamma_D(ct)$,*

where ν is the “speed” of the geodesic. This allows us to write $\text{Exp}_x(c\nu) = \gamma_\nu(c) = \gamma_{c\nu}(1)$. Recall that for Riemann geodesics we have $\|\dot{\gamma}(t)\| = \nu$ for all $t \in [0, 1]$, a constant.

Then we derive a bound for the norm of the gradients from the assumed strong convexity of f (2). Similar to the Euclidean case, the right hand side of (2) is minimized by $\text{Exp}_x^{-1}(y) = -\frac{1}{S} \nabla_x$, since the Riemann metric is positive definite, allowing us to write $f(y) \geq f(x) - \frac{1}{2S} \|\nabla_x\|^2$.

We also bound the expectation of the variance-reduced gradient ν_t^{s+1} as follows:

$$\mathbb{E} \|\nu_t^{s+1}\|^2 \leq 4L(f(x_t^{s+1}) - 2f(x^*) + f(x^s)).$$

This bound has been proven in the Euclidean case in [12] and the Riemann case (under the aforementioned assumptions) by [22]. These results enable us to claim the following:

Theorem 3.5. *Suppose we run Algorithm 1 on a convex level set on the manifold, and x^* is a unique minimizer of $f(x)$ therein. Then, under Assumptions 1 and 2, there exists an $\alpha \in (0, 1)$ s.t.*

$$\mathbb{E}(f(x^s) - f(x^*)) \leq \alpha^k \mathbb{E}(f(x_0) - f(x^*)).$$

Proof. We consider functions satisfying geodesic convexity of the form: $f(\gamma(t)) \leq (1-t)f(x) + tf(y)$ for any geodesic connecting x and y where $\gamma(0) = x, \gamma(1) = y$. Since we restrict our discussions to Riemann manifolds and metrics, the geodesics are constant speed [13].

Also assume the Riemannian gradients to be L -Lipschitz of the following form: $f(y) \leq f(x) + g_x(D, \text{Exp}_x^{-1}(y)) + \frac{L}{2} \|\text{Exp}_x^{-1}(y)\|^2$. Here $g_x(\cdot, \cdot)$ is the inner product corresponding to the Riemannian metric, and $D \in T_x \mathcal{M}$ denotes an R-gradient. We also assume bounds on the Hessian, both D^2 and the Lax-Milgram representation, similar to the ones in [18].

The expectation of the variance-reduced gradient ν_t can be bounded as follows (see [22] for a proof):

$$\mathbb{E}\|\nu_t^{s+1}\|^2 \leq 4L(f(x_t^{s+1}) - 2f(x^*) + f(x^s)).$$

We assume the function to be S -“strongly” convex on the manifold in the following sense:

$$f(y) \geq f(x) + g_x(D, \text{Exp}_x^{-1}(y)) + \frac{S}{2}\|\text{Exp}_x^{-1}(y)\|^2.$$

Note the analogy with the Euclidean case and how this condition together with the L -Lipschitz gradient restriction allows a convenient bracket for the pair of function values at any arbitrary $x, y \in \mathcal{M}$.

Using these conditions we arrive at the following lemma (new proof, quad approximation..., Riesz representation relating D and ∇): $f(x) - f(x^*) \leq \frac{1}{2L}\|\nabla f(x)\|^2$. This condition has appeared in the literature under the “gradient-dominated” moniker. Also recall the retraction formula: $x_{t+1}^{s+1} = \text{Exp}_{x_t^{s+1}}(-\eta H_r^{s+1} \nu_t^{s+1})$.

The convergence result can be stated as:

$$\mathbb{E}(f(x_k) - f(x^*)) \leq \alpha^k \mathbb{E}(f(x_0) - f(x^*)),$$

where the constants in the algorithm (the constant learning rate, inner loop iteration count) are chosed to ensure

$$\alpha = \frac{\eta\Gamma^2\Lambda^2 + (2m\eta)^{-1}}{\gamma\lambda - \eta\Gamma^2\Lambda^2} < 1.$$

The proof is similar to the one in [15], in a Riemann setting. We omit the subscript to the Riemann metric when the location of the inner product is clear from the context. By Lipschitz continuity of the gradient, we have :

$$\begin{aligned} & f(x_{t+1}^{s+1}) \\ & \leq f(x_t^{s+1}) + g(\nabla f(x_t^{s+1}), \text{Exp}_{x_t^{s+1}}^{-1}(x_{t+1}^{s+1})) \\ & + \frac{L}{2}\|\text{Exp}_{x_t^{s+1}}^{-1}(x_{t+1}^{s+1})\|^2 \\ & = f(x_t^{s+1}) - \eta g(\nabla f(x_t^{s+1}), H_r^{s+1} \nu_t^{s+1}) \\ & + \frac{L}{2}\|\text{Exp}_{x_t^{s+1}}^{-1}(x_{t+1}^{s+1})\|^2. \end{aligned}$$

Taking expectation over the sigma algebra of all random variables seen so far, we have

$$\begin{aligned}
& \mathbb{E}f(x_{t+1}^{s+1}) \\
& \leq f(x_t^{s+1}) - \eta\gamma g(\nabla f(x_t^{s+1}), \mathbb{E}(\nu_t^{s+1})) + \frac{L}{2}\eta^2\Gamma^2\|\nu_t^{s+1}\|^2 \\
& = f(x_t^{s+1}) - \eta\gamma\|\nabla f(x_t^{s+1})\|^2 + \frac{L}{2}\eta^2\Gamma^2\mathbb{E}\|\nu_t^{s+1}\|^2 \\
& \leq f(x_t^{s+1}) - 2\eta\gamma L \cdot \mathbb{E}(f(x_t^{s+1}) - f(x^*)) \\
& \quad + 2\eta^2\Gamma^2 L \cdot \mathbb{E}(f(x_t^{s+1}) + f(x^s) - 2f(x^*)) \\
& = f(x_t^{s+1}) - [2\eta\gamma L - 2\eta^2\Gamma^2 L^2]\mathbb{E}(f(x_t^{s+1}) - f(x^*)) \\
& \quad + 2\eta^2\Gamma^2 L^2(f(x^s) - f(x^*)).
\end{aligned}$$

Summing over the t and taking expectations, we have

$$\begin{aligned}
& \mathbb{E}f(x^{s+1}) \\
& \leq \mathbb{E}f(x^s) - 2\eta L[\gamma - \eta\Gamma^2 L][mf(x^{s+1}) - mf(x^*)] \\
& \quad + 2\eta^2\Gamma^2 L^2 m \cdot \mathbb{E}(f(x^s) - f(x^*)).
\end{aligned}$$

Now since $f(x^*) < f(x^{s+1})$, we have

$$\begin{aligned}
& \mathbb{E}f(x^*) \\
& \leq \mathbb{E}f(x^s) - 2\eta L[\gamma - \eta\Gamma^2 L]\mathbb{E}[mf(x^{s+1}) - mf(x^*)] \\
& \quad + 2\eta^2\Gamma^2 L^2 m \cdot \mathbb{E}(f(x^s) - f(x^*)).
\end{aligned}$$

which gives upon rearranging gives us the following bound

$$\mathbb{E}(f(x^{s+1}) - f(x^*)) \leq \frac{1 + 2\eta^2\Gamma^2 L^2 m}{2\eta m L(\gamma - \eta\Gamma^2 L)} \mathbb{E}(f(x^s) - f(x^*)).$$

Iterating the outer loop for $s = 1, \dots, k$, we have the required convergence result, where $\alpha = \frac{1 + 2\eta^2\Gamma^2 L^2 m}{2\eta m L(\gamma - \eta\Gamma^2 L)}$. \square

4 Variance-reduced stochastic RTR

The stochastic L-BFGS algorithm described above does exhibit linear convergence for strongly convex problems on the manifold as we show in the experiments, but it has some issues with scaling to high learning rates. For instance, in our synthetic experiments on computing Karcher means of p.s.d. matrices, the error decay rate does not noticeably improve if we increase the learning rate from the order of $1e-4$ to $1e-1$, whereas a minibatched version of Riemannian SVRG shows noticeably better scaling ability, losing out to the algorithm above only for rates on the order of $1e-5$ or lower. Moreover, for nonconvex settings on the manifold, global convergence cannot be guaranteed, since the lower bounds on the eigenvalues of the Hessian estimates that we assume in the convergence proof do not necessarily hold. Of course, local convergence

is still a possibility, as we see in Figure 2, where the algorithm finds a region of lower error for the PCA problem faster than rSVRG, ostensibly due to the initial search region being locally convex, but starts getting misdirected soon thereafter.

We therefore propose a second algorithm, a Riemannian trust-region method similar to [1, 2] augmented with stochastic variance-reduced gradient steps similar to the ones discussed so far. As we will see in the experiments, this algorithm performs noticeably better than rSVRG in all our experiments. A more interesting observation is the fact that the VR steps help it beat a well-tuned implementation of the RTR algorithm from [2] in some of our experiments.

4.1 The Algorithm

The basic idea is to accelerate the standard manifold trust region algorithm with stochastic variance-reduction steps. Our first approach was to use the stochastic VR gradients to approximately solve the trust region subproblem. However this method could only guarantee local convergence, and performed only slightly better than the BFGS-based algorithm above for real datasets. We address this issue with Algorithm 2, where the trust region corrections occur after one pass over the dataset using VR gradients. Although this introduces one additional pass over the full data to calculate the gradient in step 11, and potentially more depending on the formulation of the Hessian approximation used to solve (5) below, in our experiments we found it to have the best convergence speed among the manifold optimization algorithms in terms of total number of data passes, and completely outperform them in terms of number of epochs required to attain very low log-error rates.

Similar to the basic RTR procedure, the trust-region subproblem solved by our algorithm can be formulated as

$$\eta_t = \arg \min_{\eta \in T_{x_t} \mathcal{M}} \left(f(x_t) + f(\text{grad} f(x_t), \eta) + \frac{1}{2} g(\mathcal{H}_{x_t} \eta, \eta) \right), \quad (5)$$

s.t. $\|\eta\|^2 \leq \Delta_t^2$. Here $\mathcal{H}_{x_t} : T_{x_t} \mathcal{M} \rightarrow T_{x_t} \mathcal{M}$ is some linear operator on the tangent space, for example a Hessian, and Δ_t denotes the trust region radius. As shown in line [xx] of the algorithm, we set our retraction to be $x_{t+1}^{s+1} = \text{Exp}_{x_t^{s+1}}(\eta_t)$. Denoting the trust region objective function in (5) by $Y_{x_t}(\eta)$, the acceptance control variable is calculated as

$$\rho_t = \frac{f(x_t^{s+1}) - f(\text{Exp}_{x_t^{s+1}}(\eta_t))}{Y_{x_t^{s+1}}(0_{x_t^{s+1}}) - Y_{x_t^{s+1}}(\eta_t)}. \quad (6)$$

We use Algorithm 11 from [2] to approximate a solution to this in step 12. Prior to doing so, we compute another full gradient in step 11 using the last iterate from the preceding VR loop, and use them as initializations to the subroutine for solving (5). If the reduction in the objective is sufficiently large, we apply a retraction to the output of this subroutine to get our iterate for the current epoch, else we set the latter to the last iterate of the VR loop. The heuristics for updating the trust region control variate are shown in the pseudocode is shown in Algorithm 2.

As we show in the experiments, this algorithm exhibits superlinear convergence for strongly convex problems on the manifold. Intuitively, this behavior is easy to

Algorithm 2 Stochastic VR-RTR

1: **Input:** Initial value x^0 , learning rate η , batch size b_m , $\bar{\Delta} > 0$, $\Delta_0 \in (0, \bar{\Delta})$, $\hat{\rho} \in [0, 0.25)$.
2: **for** $s = 0, 1, \dots$ **do**
3: Set $x_0 = x^s$;
4: Compute full gradient $g = N^{-1} \sum_{i=1}^N \nabla f_i(x^s)$;
5: **for** $t = 0, 1, \dots, m - 1$ **do**
6: Sample minibatch $I_{b_m} \subset 1, \dots, N$;
7: Compute $\tilde{\nabla} f(x_t)$ and $\tilde{\nabla} f(x^s)$ using I_{b_m} ;
8: Set $\nu_t^{s+1} = \tilde{\nabla} f(x_t) - \Gamma_\gamma(\tilde{\nabla} f(x^s) - g)$;
9: Set $x_{t+1} = \text{Exp}_{x_t}(-\eta \nu_t^{s+1})$;
10: **end for**
11: Compute full gradient $g^t = N^{-1} \sum_{i=1}^N \nabla f_i(x_m)$;
12: Solve subproblem in (5) for η_t , with $\text{grad}f(\cdot) = g^t$;
13: Compute ρ_t from (6) using η_t ;
14: **if** $\rho_t < 0.25$ **then**
15: $\Delta_{t+1}^{s+1} = 0.25 \Delta_t^{s+1}$;
16: **else if** $\rho_t > 0.75$ & $\|\eta_t\| = \Delta_t^{s+1}$ **then**
17: $\Delta_{t+1}^{s+1} = \min(2\Delta_t^{s+1}, \bar{\Delta})$;
18: **else**
19: $\Delta_{t+1}^{s+1} = \Delta_t^{s+1}$;
20: **end if**
21: **if** $\rho_t > \hat{\rho}$ **then**
22: Set $x^{s+1} = \text{Exp}_{x_m}(\eta_t)$;
23: **else**
24: Set $x^{s+1} = x_m$;
25: **end if**
26: Set $\Delta_0^{s+1} = \Delta_m^s$;
27: **end for**

see; the variance reduced steps in lines 4 through 10 are known to provide a globally convergent sequence of iterates under standard assumptions of Lipschitz continuity for the gradients. Moreover, as mentioned in [1], the approximate solutions to (5) are guaranteed to yield a reduction in the objective function value, as well as lead to vanishing gradients in the limit, under standard Lipschitz assumptions. We verify this behavior in the next section, where the algorithm performs better than both a minibatch version of SVRG and the RTR technique in our experiments, in terms of number of passes over data required for convergence. We leave a formal analysis of convergence to future work.

5 Experiments

5.1 Karcher mean computation for PSD matrices

We begin with a synthetic experiment on learning the Karcher mean [3] of positive definite matrices. We compare four algorithms: a minibatched variant of the Riemannian SVRG algorithm from [22], the stochastic variance-reduced L-BFGS procedure from Algorithm 1, the RTR-augmented stochastic technique from Algorithm 2, as well as the full-data Riemannian trust-region method described in [2]. We implemented all the stochastic algorithms using the Manopt toolkit¹, and used the implementation therein for RTR. We call these four algorithms rSVRG, rSV-LBFGS, SV-RTR and RTR respectively. For both Algorithm 2 and RTR, we use Algorithm 11 from [2] for computing an approximate solution to (5). We capped the number of iterations in this procedure to three. In practice, we observed both RTR and our algorithm to execute an average of two of these inner iterations per epoch.

We generated three sets of 1000 random positive definite matrices, each of size 100×100 , with condition numbers 10, $1e3$, and $1e5$, using code from [4] to calculate the ground truth as well. We used a batchsize of 50 for all stochastic algorithms, and initialized all four with the same initial matrix. We observed the rSVRG algorithm to scale well with learning rate in this problem, ostensibly due to the strong convexity on the manifold; hence we used a fixed learning rate of 0.1 for both rSVRG and SV-RTR. Our LBFGS-based technique however was generally unable to scale similarly beyond the first couple of epochs; to avoid convergence issues we used a learning rate of 0.01 for this method. We plot the log-errors vs the number of passes over the full dataset in Fig.1.

As shown in the plot, for all three condition numbers the SV-RTR algorithm exhibits noticeably better convergence behavior than both rSVRG and rSV-LBFGS. In fact, our trust-region augmentation step helps the SV-RTR algorithm beat the RTR algorithm as well, most noticeably for condition numbers 10 and $1e5$. We attribute this behavior to the strong convexity of the cost function, which allows us to leverage the robust convergence rate of linear variance-reduced techniques using a high learning rate. We believe this to be a key takeaway from this experiment. The augmentation also helps SV-RTR perform better than the remarkably robust rSVRG technique. Our BFGS-based algorithm apparently gets stuck in some local mode, in spite of performing similarly to the other two stochastic methods for the first few epochs.

5.2 Leading eigenvalue computation

Next we conduct a synthetic experiment on calculating the leading eigenvalue of symmetric matrices, for example data covariance matrices. This is clearly a common problem in machine learning, and as such is a unit-norm constrained nonconvex optimization problem in Euclidean space. We therefore can transform this into an unconstrained manifold optimization problem on the sphere defined by the norm constraint. To that end, we again generate three sets of datapoints, for eigengaps 0.005, 0.01 and 0.1, using the techniques described in [20]. Each dataset contains 100,000 datapoints, each

¹<http://www.manopt.org>

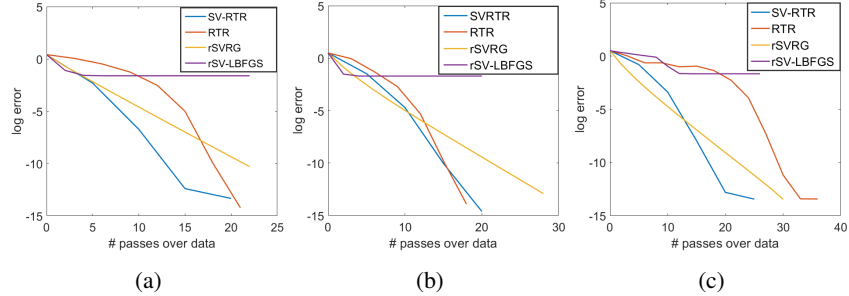


Figure 1: Error decay plots for SV-RTR, rSVRG, rSV-LBFGS, and RTR obtained from the three synthetic Karcher mean computation experiments. Figures (a), (b) and (c) show the log-errors for datasets with condition numbers 10 , $1e3$ and $1e5$ respectively, plotted against number of passes over full dataset for each algorithm. See text for experimental details.

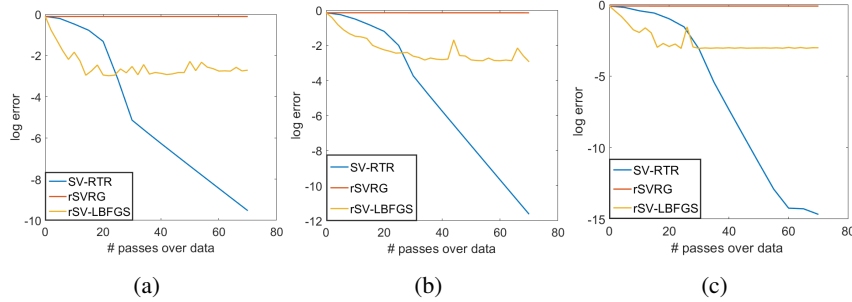


Figure 2: Error decay plots for SV-RTR, rSVRG, rSV-LBFGS, and RTR obtained from the three synthetic dominating eigenvalue computation experiments. Figures (a), (b) and (c) show the log-errors for datasets with eigengaps 0.005 , 0.01 and 0.1 respectively, plotted against number of passes over full dataset for each algorithm. See text for experimental details.

of dimension 1000. We compare the performance of the two algorithms proposed in this paper with rSVRG. We used batchsizes of 800, 900, and 900, selected using grid-search, for the datasets with eigengaps 0.005 , 0.01 and 0.1 respectively. For rSVRG and SV-RTR, we used a learning rate of 0.1 , and 0.01 for rSV-LBFGS. The results are shown in Fig.2. SV-RTR performs significantly better than the other two stochastic algorithms.

The results are somewhat different from the previous synthetic case, in that rSVRG does not scale as robustly with learning rate as it did for the strongly convex problem above. The log-error decay was linear, but the other two algorithms performed noticeably better. The performance of rSV-LBFGS was similarly slow for smaller values of the learning rate, but as shown, it scales somewhat better. We believe that using a

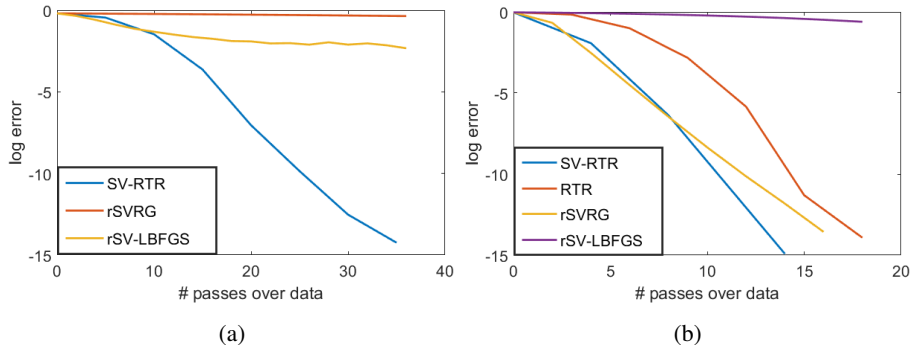


Figure 3: Error decay plots for SV-RTR, rSVRG, and rSV-LBFGS obtained for dominating eigenvalue computation on the MNIST and RCV1 data matrices, showing log-error versus number of passes over dataset. See text for experimental details.

decay factor for the learning rate might help in smoothing out the observed error plot, without any issues with the convergence analysis. We also ran RTR on this dataset, but its performance closely followed that of SV-RTR, similar to the behavior shown in Fig.1b above. The performance of VR-PCA [20] was significantly better than SV-RTR for an eigengap of 0.1, and almost identical for the others.

5.3 Eigenvalue computation for real data matrices

Finally, we perform leading eigenvalue computations for two real matrices, MNIST and RCV1. For MNIST we used all 70,000 datapoints for a total matrix size of 784×70000 . For RCV1 we have a vocabulary of 10,000 words and 704,414 training documents and 10,000 test documents. We concatenated the training and test word counts for a total matrix size of 10000×804414 . The rest of the experimental setup was identical to the synthetic setup above; we used batchsizes of 100 and 500, and learning rates of 0.01 and 0.0001 for MNIST and RCV1 respectively. As with the synthetic experiments in the previous section, we used the output of Matlab’s *eig* and *eigs* functions as our ground truth. The results are shown in Figures 3a,3b. As with the synthetic dataset, we observed slow convergence for the minibatched rSVRG, and relatively better performance by rSV-LBFGS for MNIST. For RCV however, the first order method performed noticeably better, keeping up with SV-RTR for the first few passes over the data. SV-RTR was the fastest to reach very low error rates in both cases, even beating the RTR method for the RCV dataset.

Regarding the learning rates, one should be able to get better performance from all the algorithms here by individually tuning the rates. The authors in [22], for instance, use curvature assumptions in their calculation of a suitable learning rate. We opted for using equal rates for all three for a more direct comparison, since we believe that robust scaling with high learning rates is a desirable feature for these algorithms. We also should note that the number of passes over the data in each epoch differ among

the four algorithms; for rSVRG and rSV-LBFGS, we have two passes per epoch, for RTR and SV-RTR we observed an average of two inner iterations (to solve (5)) in each epoch. In each of these inner iterations we computed an approximate Hessian using one pass over the data; this led to an average of three passes per epoch for RTR and five for SV-RTR. This further emphasizes the superior convergence behavior of SV-RTR; it required very few epochs (~ 5 for the real datasets) to attain low learning rates; in fact it was competitive with the very fast VR-PCA procedure in terms of number of epochs in the latter experiments. However, since VR-PCA only performs two passes per epoch, it was faster overall. Clearly, executing fewer inner iterations and/or finding better ways to approximate the Hessian for the trust-region subproblem would lead to even higher improvement for our method relative to existing manifold methods, and would be an interesting avenue for further investigation in its own right.

6 Conclusion

We propose novel stochastic L-BFGS and trust-region algorithms on Riemann manifolds with variance reduction augmentations for the stochastic gradients, and provide convergence analyses for manifold convex functions for the former. Our trust region-based algorithm exhibits noticeably better performance than recently proposed first-order stochastic Riemannian optimization algorithms for computation of Karcher means and leading eigenvectors of symmetric positive definite matrices, both for synthetic and real data experiments.

References

- [1] P.-A. Absil, C. G. Baker, and K. A. Gallivan. Trust-region methods on Riemannian manifolds. *Found. Comput. Math.*, 7(3):303–330, July 2007.
- [2] P. A. Absil, R. Mahony, and R. Sepulchre. *Optimization Algorithms on Matrix Manifolds*. Princeton University Press, 2008.
- [3] R. Bhatia. *Positive Definite Matrices*. Princeton University Press, 2007.
- [4] D. A. Bini and B. Iannazzo. Computing the Karcher mean of symmetric positive definite matrices. *Linear Algebra and its Applications*, 483(4):1700–1710, 2013.
- [5] S. Bonnabel. Stochastic gradient descent on Riemannian manifolds. *IEEE Transactions on Automatic Control*, 58(9):2217–2229, 2013.
- [6] W. M. Boothby. *An Introduction to Differentiable Manifolds and Riemannian Geometry*. Academic Press Inc., 1986.
- [7] L. Bottou. Large-scale machine learning with stochastic gradient descent. In *International Conference on Computational Statistics*, 2010.
- [8] L. Bottou and Y. LeCun. Large scale online learning. In *NIPS*, 2004.

- [9] S. Bubeck. Convex Optimization: Algorithms and Complexity. *Foundations and Trends in Machine Learning*, 8(3–4):231–357, 2015.
- [10] R. H. Byrd, S. L. Hansen, J. Nocedal, and Y. Singer. A Stochastic Quasi-Newton Method for Large-scale Optimization, 2014. arXiv:1410.1068.
- [11] R. Hosseini and S. Sra. Matrix Manifold Optimization for Gaussian Mixtures. In *NIPS*, 2015.
- [12] R. Johnson and T. Zhang. Accelerating Stochastic Gradient Descent using Predictive Variance Reduction. In *NIPS*, 2013.
- [13] J. Lee. *Riemann Manifolds: an Introduction to Curvature*. Springer-Verlag, 1997.
- [14] D. C. Liu and J. Nocedal. On the limited memory BFGS method for large scale optimization. *Mathematical Programming*, 45(1–3):503–528, 1989.
- [15] P. Moritz, R. Nishihara, and M. I. Jordan. A Linearly-Convergent Stochastic L-BFGS Algorithm. In *AISTATS*, 2016.
- [16] J. Nocedal and S. J. Wright. *Numerical Optimization*. Springer, 2006.
- [17] E. Oja. Principal components, minor components, and linear neural networks. *Neural Networks*, 5(6):927–935, 1992.
- [18] W. Ring and B. Wirth. Optimization methods on Riemannian manifolds and their application to shape space. *SIAM Journal on Optimization*, 22(2):596–627, 2012.
- [19] H. Robbins and S. Monro. A Stochastic Approximation Method. *The Annals of Mathematical Statistics*, 22(3):400–407, 1951.
- [20] O. Shamir. A Stochastic PCA and SVD Algorithm with an Exponential Convergence Rate. In *ICML*, 2015.
- [21] S. Sra and R. Hosseini. Conic geometric optimization on the manifold of positive definite matrices. *SIAM Journal on Optimization*, 25(1):713–739, 2015.
- [22] H. Zhang, S. J. Reddi, and S. Sra. Fast stochastic optimization on Riemannian manifolds. In *NIPS*, 2016.